# Highly Enantiomerically Enriched Secondary Alcohols via Epoxide Hydrogenolysis

Olivia J. Borden, Benjamin T. Joseph, Marianna C. Head, Obsidian Ammons, Diane Eun Kim, Abigail C. Bonino, Jason M. Keith*, and Anthony R. Chianese*

Department of Chemistry, Colgate University, 13 Oak Drive, Hamilton, New York 13346, United States

## Abstract

In this paper, we report the development of ruthenium-catalyzed hydrogenolysis of epoxides to selectively give the branched (Markovnikov) alcohol products. In contrast to previously reported catalysts, the use of Milstein's PNN-pincer-ruthenium complex at room temperature allows the conversion of enantiomerically enriched epoxides to secondary alcohols without racemization of the product. The catalyst is effective for a range of aryl epoxides, alkyl epoxides and glycidyl ethers, and is the first homogenous system to selectively promote hydrogenolysis of glycidol to 1,2-propanediol without loss of enantiomeric purity. A detailed mechanistic study was conducted, including experimental observations of catalyst speciation under catalytically relevant conditions, comprehensive kinetic characterization of the catalytic reaction, and computational analysis via density functional theory. Heterolytic hydrogen cleavage is mediated by the ruthenium center and exogenous alkoxide base. Epoxide ring-opening occurs through opposite-side attack of the ruthenium hydride on the less-hindered epoxide carbon, giving the branched alcohol product selectively.

## Introduction

The homogeneous transition-metal-catalyzed hydrogenolysis of epoxides, first reported by Ikariya and co-workers in 2003,[1] has recently emerged as a method for the selective synthesis of a variety of substituted primary, secondary, and tertiary alcohols (Scheme 1). Several reported catalysts selectively give the linear (anti-Markovnikov) alcohol isomer. For example, Scheuermann and coworkers described a PCP-pincer-iridium/triflic acid catalyst system,[2] which they later showed operates via initial acid-catalyzed hydrolysis of the epoxide, followed by hydrogenolysis to the terminal alcohol catalyzed by iridium nanoparticles generated in situ.[3] Yao et al. disclosed a titanium-cobalt dual-catalyst system, and provided evidence for a radical-based activation of $H_2$ and transfer to epoxide substrates.[4] Beller and coworkers reported an iron/trifluoroacetic acid system[5] and a cobalt/zinc triflate system,[6] both of which operate through initial Meinwald rearrangement of the epoxide to the aldehyde, followed by metal-catalyzed hydrogenation to the primary alcohol.

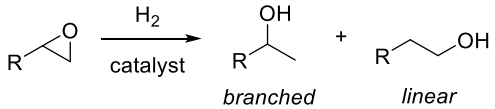


**Scheme 1.** Catalytic epoxide hydrogenolysis.

On the other hand, several catalysts selectively produce the branched (Markovnikov) alcohol isomer. So far, all reported catalysts in this category are capable of Noyori-type[7] metal-ligand

cooperation, involving either RuH/NH or FeH/OH moieties (Chart 1). Ikariya's 2003 report[1] featured a combination of Cp*RuCl(1,5-cyclooctadiene), $PPh_2CH_2CH_2NH_2$, and KOH. Gunanathan reported that the commercially available Ru-MACHO, in combination with $KO^tBu$, promotes the selective hydrogenolysis of a variety of substituted epoxides to give the Markovnikov product.[8] In both cases, the authors proposed that the epoxide ring opens through a Noyori-type concerted transfer of Ru-H and N-H to the epoxide C and O atoms, respectively. Tadiello et al. showed that a Knölker-type iron-cyclopentadienone catalyst selectively gives the linear product if $Al(OTf)_3$ is added as cocatalyst, while the branched product is favored with $Zr(O^iPr)_4$ as cocatalyst.[9] Based on DFT calculations, these authors proposed a competition between a Noyori-type concerted pathway and an initial Meinwald isomerization to the aldehyde followed by aldehyde hydrogenation.

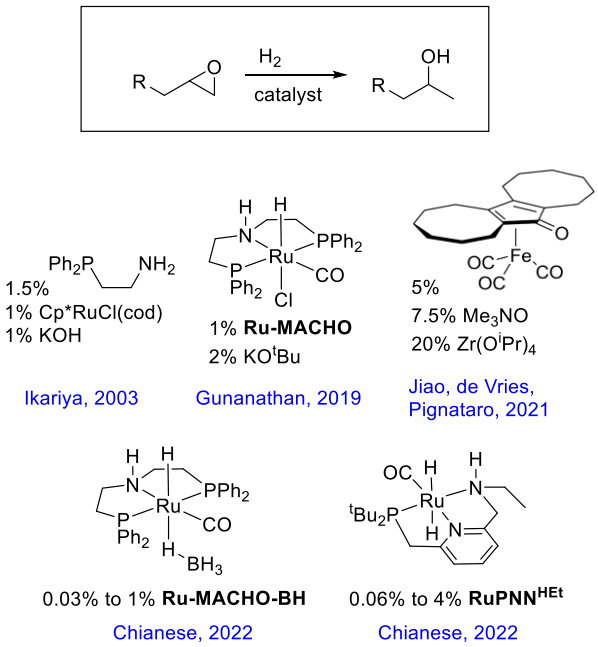


**Chart 1.** Previously reported catalysts for branched-selective epoxide hydrogenolysis.

Notably, none of the above studies describe the synthesis of enantiomerically enriched alcohols via the hydrogenolysis of enantiomerically enriched epoxides. Ikariya and coworkers noted in a 2007 review[10] that racemization of the secondary alcohol products was rapid and prevented the application of epoxide hydrogenolysis to the synthesis of enantiomerically enriched secondary alcohols. Gunanathan reported that attempted hydrogenolysis of (*R*)-glycidol gave a complex mixture of products, and did not describe other attempts with enantiomerically enriched substrates.[8]

In 2022, we reported[11] that two Noyori-type ruthenium catalysts, the commercially available **Ru-MACHO-BH** and **RuPNN$^{HEt}$**, formed from Milstein's catalyst[12] by ethane loss and hydrogen addition,[13] are highly active for the branched-selective hydrogenolysis of epoxides, without the requirement of strongly basic or Lewis-acidic cocatalysts (Chart 1). High yields were obtained at catalyst loadings as low as 0.03%, compared with 1%[1, 8] or 5%[9] loading in prior reports. Through monitoring of the reactant and

product e.e. over the course of the reaction, we showed that product racemization is rapid under the catalytic conditions, which prevented the application of this method for the synthesis of enantiomerically enriched alcohols from epoxides.

In 2023, we completed a combined experimental/computational mechanistic study of the **Ru-MACHO-BH** and **RuPNN$^{HEt}$** catalysts for epoxide hydrogenolysis.[14] For both catalysts, we showed that the previously proposed[1, 8-9] concerted, Noyori-type mechanisms for hydrogen transfer to the epoxide have implausibly high free-energy barriers in excess of 50 kcal/mol. Instead, epoxide ring-opening proceeds through $S_N2$-like opposite-side attack of the ruthenium hydride on the less-substituted epoxide carbon, *without involvement of the pendant N-H group* (Scheme 2, right). Hydrogen activation proceeds by Noyori-type metal-ligand cooperation, assisted by an alcohol functioning as a proton shuttle (Scheme 2, left).

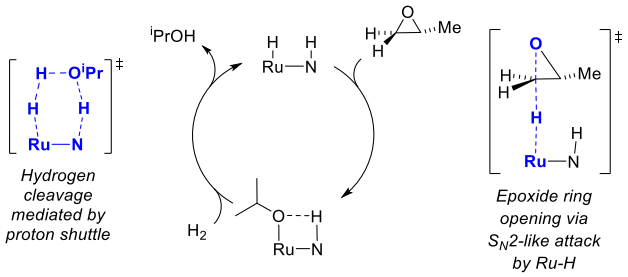


**Scheme 2.** Abbreviated mechanism for branched-selective epoxide hydrogenolysis catalyzed by Noyori-type ruthenium-pincer complexes.

Because product racemization presumably proceeds through reversible dehydrogenation of the secondary alcohol to the ketone via a Noyori-type bifunctional mechanism,[7] we hypothesized that an analogous complex lacking the pendant N-H group could potentially catalyze epoxide hydrogenolysis while avoiding product racemization. Following an extensive process of screening and optimization, we were pleased to find that the commercially available Milstein's catalyst, in combination with KO$^t$Bu or KO$^i$Pr in $^i$PrOH, promotes the hydrogenolysis of a range of substituted epoxides at room temperature, with extremely high branched:linear selectivity and minimal product racemization. This article describes the discovery and optimization of this catalyst system, an exploration of the substrate scope, and a detailed mechanistic study combining computation, kinetics, and spectroscopic analysis of resting state speciation. We conclude that epoxide ring-opening proceeds through $S_N2$-like attack of the ruthenium hydride on the less-hindered epoxide carbon, while heterolytic hydrogen activation is mediated by exogenous alkoxide base.

## Catalyst Screening and Optimization

We began our screening process with the following goals: 1) high yields of alcohol products with low catalyst loading under mild conditions; 2) high selectivity for the branched (chiral) product over the linear product; and 3) minimal racemization of the branched product. For catalyst screening, we chose

(*R*)-styrene oxide as the model substrate, because it is available commercially with 98% e.e., and because achieving high selectivity for the branched product has been challenging with aryl epoxide substrates.[1, 8-9, 11] We began by screening a variety of known transition-metal pincer complexes (Ru, Ir, and Mn). We used preformed catalysts instead of an in-situ combination of ligand and metal precursor, to avoid potential side reactions arising from incomplete metalation. Because the solvent has been shown to strongly affect both catalyst activity and selectivity in epoxide hydrogenolysis,[11] we screened catalyst systems in toluene, $^{t}$AmOH, $^{i}$PrOH, EtOH, and MeOH. Table 1 shows highlighted experiments from this optimization process; Table S1 in the Supporting Information shows the results of all 104 screening experiments conducted.

**Table 1.** Catalyst Screening and Optimization

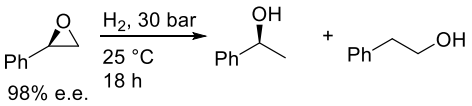


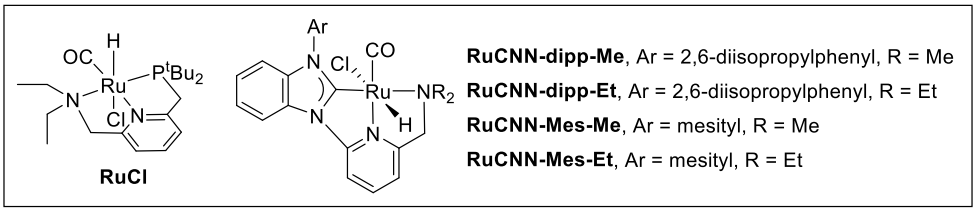


| Entry | Catalyst | mol % | Additive | mol % | Solvent | [epoxide] (M) | Yield (%) | e.e. (%) | b:l |
|---|---|---|---|---|---|---|---|---|---|
| 1 | RuCNN-dipp-Me | 1 | NaO$^t$Bu | 10 | $^i$PrOH | 0.125 | 74 | 92 | 7.4 |
| 2 | RuCNN-dipp-Et | 1 | NaO$^t$Bu | 10 | $^i$PrOH | 0.125 | >99 | 79 | 7.7 |
| 3 | RuCNN-Mes-Me | 1 | NaO$^t$Bu | 10 | $^i$PrOH | 0.125 | 79 | 91 | 5.5 |
| 4 | RuCNN-Mes-Et | 1 | NaO$^t$Bu | 10 | $^i$PrOH | 0.125 | 62 | 92 | 5.2 |
| 5 | RuCl | 1 | NaO$^t$Bu | 10 | $^i$PrOH | 0.125 | 31 | 98 | 11.1 |
| 6 | RuCl | 1 | NaO$^t$Bu | 10 | toluene | 0.125 | 2 | 98 | >10 |
| 7 | RuCl | 1 | NaO$^t$Bu | 10 | $^t$AmOH | 0.125 | 62 | 93 | 19.1 |
| 8 | RuCl | 1 | NaO$^t$Bu | 10 | EtOH | 0.125 | 3 | 98 | 6.7 |
| 9 | RuCl | 1 | none | -- | $^i$PrOH | 0.125 | 0 | -- | -- |
| 10 | RuCl | 1 | CsF | 10 | $^i$PrOH | 0.125 | 0 | -- | -- |
| 11 | RuCl | 1 | $Cs_2CO_3$ | 10 | $^i$PrOH | 0.125 | 24 | 98 | 11.5 |
| 12 | RuCl | 1 | KF | 10 | $^i$PrOH | 0.125 | 3 | -- | 0 |
| 13 | RuCl | 1 | BEMP | 10 | $^i$PrOH | 0.125 | 4 | 96 | 9.5 |
| 14 | RuCl | 1 | $LiAlH_4$ | 10 | $^i$PrOH | 0.125 | 3 | 98 | 11.6 |
| 15 | RuCl | 1 | $NaBH_4$ | 10 | $^i$PrOH | 0.125 | 5 | 93 | 5.1 |
| 16 | RuCl | 1 | KOAc | 10 | $^i$PrOH | 0.125 | 0 | -- | -- |
| 17 | RuCl | 1 | $K_3PO_4$ | 10 | $^i$PrOH | 0.125 | 8 | 98 | 9.5 |
| 18 | RuCl | 1 | KO$^t$Bu | 10 | $^i$PrOH | 0.125 | 57 | 98 | 11.3 |
| 19 | RuCl | 0.25 | KO$^t$Bu | 10 | $^i$PrOH | 0.5 | 36 | 98 | 12.2 |
| **20** | **RuCl** | **1** | **KO$^t$Bu** | **2.5** | **$^i$PrOH** | **0.5** | **>99** | **98** | **11.9** |
| 21 | RuCl | 1 | KO$^t$Bu | 10 | $^i$PrOH | 0.5 | >99 | 98 | 12 |
| 22 | RuCl | 1 | LiO$^i$Pr | 2.5 | $^i$PrOH | 0.5 | 52 | 98 | 11.9 |
| 23 | RuCl | 1 | NaO$^i$Pr | 2.5 | $^i$PrOH | 0.5 | 60 | 98 | 12.0 |
| **24** | **RuCl** | **1** | **KO$^i$Pr** | **2.5** | **$^i$PrOH** | **0.5** | **>99** | **98** | **11.9** |

Entries 1-5 show the most promising precatalysts identified in our screening. Notably, all five are ruthenium-pincer complexes, where the pincer ligand lacks an N-H functional group. Of these complexes, we identified Milstein's hydridochloride precatalyst **RuCl** (Entry 5) as the most promising, because it provided the highest branched:linear selectivity and showed no observable product racemization. Switching the solvent from isopropyl alcohol (Entry 5) to toluene (Entry 6) or ethanol (Entry 8) dramatically decreased the product yield. Catalyst activity was improved in *t*-amyl alcohol

(Entry 7), but some product racemization was observed in this solvent. Continuing with **RuCl** in isopropyl alcohol, we then screened a variety of basic or hydridic additives (Entries 9-18). In this series, KO$^t$Bu (Entry 18) emerged as the most promising additive, providing the alcohol product in 57% yield with high branched selectivity and no observable product racemization. We then surveyed a range of substrate, catalyst, and base concentrations (Entries 19-21), and found the following: 1) higher epoxide concentration is beneficial; 2) 1 mol % loading of **RuCl** is necessary for full conversion; and 3) the loading of KO$^t$Bu can be lowered to 2.5 mol % with no decrease in yield or selectivity.

The improved yield with KO$^t$Bu compared to NaO$^t$Bu (Entries 5 vs. 18) prompted a comparison of the effect of the alkali metal cation. To avoid complexities arising from multiple alcohols and alkoxide anions in the isopropyl alcohol solvent, we compared the commercially available salts of isopropoxide (Entries 22-24). We found that KO$^i$Pr was as effective as KO$^t$Bu (Entries 24 vs. 20), but that NaO$^i$Pr and LiO$^i$Pr were less effective, giving similar selectivities but decreased conversion to product. In the end, Entries 20 and 24 represent the optimized conditions for this reaction, giving >99% yield of phenethyl alcohol with no observable racemization and a branched:linear ratio of 11.9:1. For practical synthetic applications, KO$^t$Bu is preferred as base because of its commercial availability as a solid. KO$^i$Pr was employed in our kinetic studies described below, which were conducted in isopropyl alcohol solvent.

**Substrate Scope**

With optimized conditions determined for epoxide hydrogenolysis catalyzed by **RuCl** and KO$^t$Bu, we began to survey the reactivity of a variety of monosubstituted epoxide substrates, to assess whether the catalyst activity, selectivity, and absence of product racemization were maintained (Table 2). First, we compared differently substituted aryl epoxides, which have posed a challenge in the past in obtaining a high regioselectivity for the branched product.[1, 8, 11] (*R*)-Styrene oxide, the subject of the above optimization study, is reduced with 11.9:1 selectivity for the branched product, with no observable product racemization. Para-fluoro, -chloro- and -bromo substituents are all tolerated, and even higher regioselectivity for the branched product is observed. The fluoro- and bromo-substituted epoxides required a higher catalyst loading, 4% and 2% respectively, to achieve full conversion. For the chloro- and bromo-substituted epoxides, a small amount of product racemization was observed, corresponding to 3% and 2% loss of enantiomeric excess, respectively, for these substrates.

**Table 2.** Substrate Scope for Epoxide Hydrogenolysis

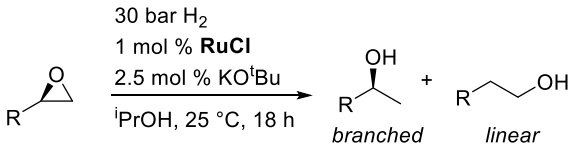


| Substrate | % Conv. | % Yield | Epoxide % e.e. | Product % e.e | b:l |
|---|---|---|---|---|---|
| 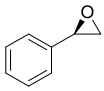 | 98 | 97 | 98 | 98 | 11.9 |
| 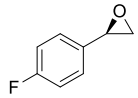 | 96 | 94[a] | 85 | 85 | 18.1 |
| 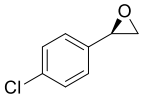 | 100 | 99 | 97 | 94 | 20.0 |
| 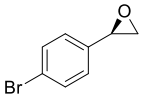 | 99 | 93[b] | >99 | 98 | 23 |
|  | 98 | 98 | >99 | >99 | >99 |
|  | 99 | 94 | >99 | >99 | >99 |
| 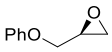 | 100 | 99 (88)[c] | >99 | >99 | >99 |
| 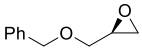 | 99 | 99 (91)[c] | >99 | >99 | >99 |
| 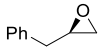 | 98 | 94 | 96 | 96 | >99 |
| 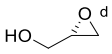 | 88 | 63[e] | >99 | >99 | >99 |

[a] 2 mol % **RuCl** and 5 mol % KO$^t$Bu were used. [b] 4 mol % **RuCl** and 10 mol % KO$^t$Bu were used. [c] Percent yields in parentheses represent isolated yields on a 1.0 gram scale. [d] (*S*)-glycidol was used as shown, and gave the (*S*)-1,2-propanediol product expected if the configuration of the stereocenter is retained. [e] 3.3 mol % **RuCl** and 8.3 mol % KO$^t$Bu were used.

We then turned to monosubstituted epoxides with a directly attached $sp^3$ carbon, which typically give only the branched product in hydrogenolysis catalyzed by Noyori-type complexes.[1, 8, 11] The aliphatic epoxides 1-octene oxide and 1-tetradecene oxide were cleanly converted to the secondary alcohols in high yield with no observable linear product and no product racemization. Similar results were obtained for phenyloxy- and benzyloxy-substituted derivatives, as well as allyl benzene oxide. The hydrogenolysis of substrates containing a primary alcohol functional group poses a particular challenge, as base-promoted oligomerization competes with hydrogenolysis at higher temperatures. Ikariya reported no substrates with alcohol functional groups,[1] and Gunanathan reported that a complex mixture was

obtained for the hydrogenolysis of (*R*)-glycidol catalyzed by **Ru-MACHO** and KO$^t$Bu.[8] With our system operating at room temperature, (*S*)-glycidol was hydrogenated to give the (*S*)-1,2-propanediol product with no loss of e.e. in 63% yield, albeit with a higher 3.3% loading of **RuCl** required to achieve high conversion.

**Mechanistic Study: Background**

Milstein's catalyst precursor **RuCl** – and the deprotonated, dearomatized form **Ru-dearom** – have a rich history of application in the hydrogenation and dehydrogenation of polar bonds,[15] following Milstein's initial reports of ester hydrogenation[16] and the reverse reaction, the acceptorless dehydrogenative coupling of primary alcohols to esters.[12] **Ru-dearom** is known to reversibly activate dihydrogen at room temperature to give the dihydride **RuH** (Scheme 3).[16] This metal-ligand-cooperative cleavage of hydrogen (or its reverse in dehydrogenation reactions) was featured in many DFT studies of the reactions catalyzed by **RuH** or **Ru-dearom**,[17] but experimental studies of catalyst speciation under operating conditions (≥ 100 °C) were not reported.

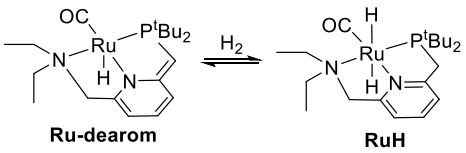


**Ru-dearom** **RuH**

**Scheme 3.** Reversible activation of hydrogen by **Ru-dearom**.

In 2019, we demonstrated that **Ru-dearom** is catalytically *inactive* for ester hydrogenation, but rapidly undergoes a dehydroalkylation reaction under the conditions of catalysis, releasing ethane and ultimately producing **RuPNN$^{HEt}$**,[13] which operates through a well-precedented Noyori-type mechanism requiring the nascent N-H functional group (Scheme 4, top).[18] Khaskin and Gusev later showed that the closely related **RuPNN$^{bpy}$** also forms a Noyori-type catalyst **RuPNN$^{pip}$** under operating conditions, this time through hydrogenation of the pyridine ring (Scheme 4, bottom).[19] In 2020, Gusev showed through DFT that for Milstein's catalyst, hydrogen activation mediated by an exogenous alkoxide ion proceeds with a lower barrier than activation through the $CH_2$ linker.[20] Taken together, these recent reports call into question the involvement of aromatization/dearomatization pathways through the $CH_2$ linkers in catalysis for complexes such as **Ru-dearom** and **RuPNN$^{bpy}$**, and emphasize that DFT calculations and studies of stoichiometric reactivity at low temperature, while informative, are most reliable when paired with experimental characterization under catalytically relevant conditions.

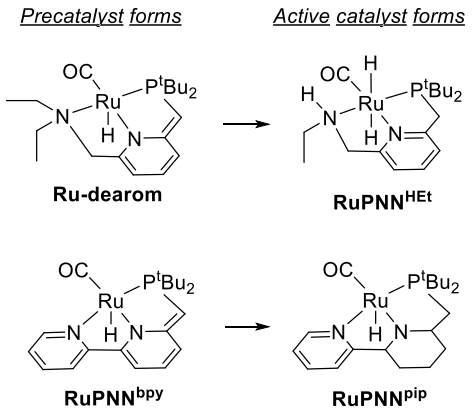


**Scheme 4.** Conversion of precatalysts with dearomatized pincer ligands to the active, Noyori-type forms.

For the present catalytic transformation, dehydroalkylative catalyst activation (Scheme 4, top) can be excluded because the reaction is conducted at 25 °C, where dehydroalkylation is known to be extremely slow.[13] Although **RuPNN$^{HEt}$**, the product of dehydroalkylative activation of **Ru-dearom**, is also known to catalyze epoxide hydrogenolysis, it also rapidly catalyzes product racemization,[11] which is not observed in this work. Based on Gusev's recent report, we expected that the most energetically accessible pathway for hydrogen activation would involve deprotonation of ruthenium-coordinated $H_2$ by exogenous alkoxide.[20] We anticipated that the preferred pathway for epoxide ring-opening by **RuH** would involve $S_N2$-like attack of the ruthenium-hydride on the less-hindered epoxide carbon, as we previously demonstrated for the closely analogous complex **RuPNN$^{HEt}$**.[14] To test these hypotheses while considering plausible alternatives, we employed a combination of spectroscopic analysis of catalyst speciation under catalytically relevant conditions, kinetic analysis, and density functional theory calculations.

## Analysis of Catalyst Resting Speciation

We began by studying the speciation of **RuCl**, activated with KO$^t$Bu, by NMR spectroscopy in isopropyl alcohol solvent under varying pressures of $H_2$. In the absence of hydrogen, the hydridoalkoxide species **RuO$^i$Pr** is formed cleanly, in agreement with previous reports.[20-21] Under hydrogen, a rapid equilibrium is established between **RuO$^i$Pr** and **RuH** (Scheme 5).

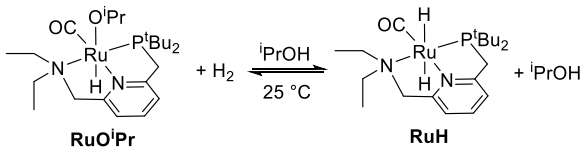


**Scheme 5.** Equilibrium between **RuO$^i$Pr** and **RuH**.

Figure 1 shows the mole fraction [**RuH**] / $[Ru]_{total}$ as a function of the hydrogen concentration, as measured by $^1$H NMR spectroscopy in nondeuterated isopropyl alcohol at 25 °C. A least-squares fit gives $K_1 = 89 \pm 6$, corresponding to $\Delta G° = -2.66 \pm 0.04$ kcal/mol (see the SI for details). The addition of 0.25 M tetradecene oxide did not produce any new ruthenium species under these conditions or alter the observed ratios, providing evidence against the involvement of additional species with a ruthenium- or ligand-bound epoxide.[22]

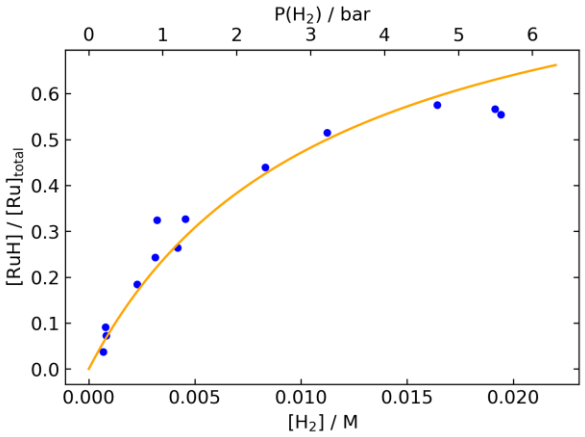


**Figure 1.** The mole fraction [**RuH**]/$[Ru]_{total}$ vs. $[H_2]$, as determined by $^1$H NMR spectroscopy. Blue points represent values measured in independent experiments. The orange curve represents the best fit of the data to determine the equilibrium constant $K_1$.

Using DFT, we calculated the free energies of the potential resting states **RuO$^i$Pr**, **RuH**, and **Ru-dearom**, in the presence and absence of explicit isopropyl alcohol solvent molecules. Scheme 6 shows the calculated relative free energies. **RuH** and **Ru-dearom** show very a small effect of explicit solvent (≤ 0.6 kcal/mol), but **RuO$^i$Pr** shows a greater effect, as **RuO$^i$Pr-solv** is 1.9 kcal/mol lower than **RuO$^i$Pr**. This is consistent with previous studies,[14, 18] and results from the strong hydrogen-bond-accepting ability of the coordinated alkoxide oxygen in **RuO$^i$Pr**. The calculated standard-state free energy change of -5.7 kcal/mol for the conversion of **RuO$^i$Pr** to **RuH** agrees well with the experimentally measured value of -2.66 kcal/mol. The absence of **Ru-dearom** in these experiments is qualitatively consistent with its higher standard-state free energy calculated by DFT.

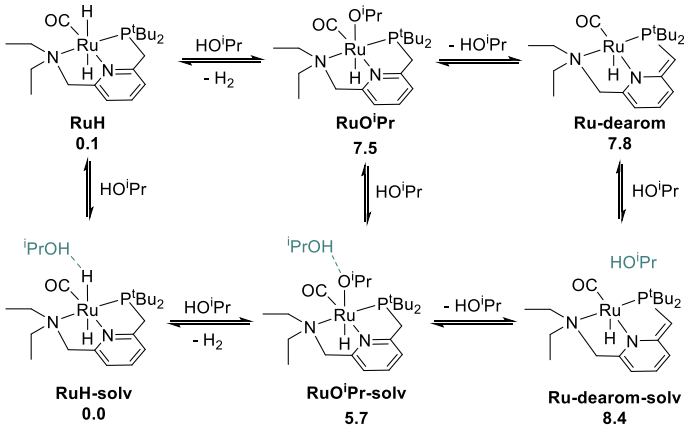


**Scheme 6.** Relative standard-state free energies of plausible catalyst resting states, calculated by DFT at 298.15 K.

## Minimum-Energy Pathway

With experimental confirmation of the resting-state speciation calculated by DFT, we turned to elucidating the pathways for hydrogen activation and epoxide ring-opening. To appropriately model the steric and electronic nature of our experimental model substrate, 1-tetradecene oxide, we chose propylene oxide as the model substrate for computations. This has the benefit of minimizing complications due to the multiple conformations of the alkyl chain in 1-tetradecene oxide. Figure 2 shows the calculated minimum-energy pathway for the hydrogenolysis of propylene oxide to isopropyl alcohol, beginning with **RuO$^i$Pr-solv**. First, alkoxide dissociation to give **a** is followed by $H_2$ coordination to give the σ-complex **b**. This species is deprotonated by exogenous isopropoxide in a nearly barrierless reaction through **c-TS**, which generates the predominant resting state **RuH-solv**. This isopropoxide-mediated hydrogen activation reaction closely follows the ethoxide-mediated pathway previously reported by Gusev.[20] **RuH-solv** then forms the dispersion adduct **d**, after which epoxide ring-opening proceeds through **e-TS**, representing an $S_N2$-like attack of the ruthenium hydride on the terminal epoxide carbon. This leads directly to the C-H σ-complex **f**, which rearranges to regenerate **RuO$^i$Pr-solv**. The epoxide ring-opening pathway from **RuH-solv** to **RuO$^i$Pr-solv** is analogous to that calculated previously for the very similar complex **RuPNN$^{HEt}$**.[14]

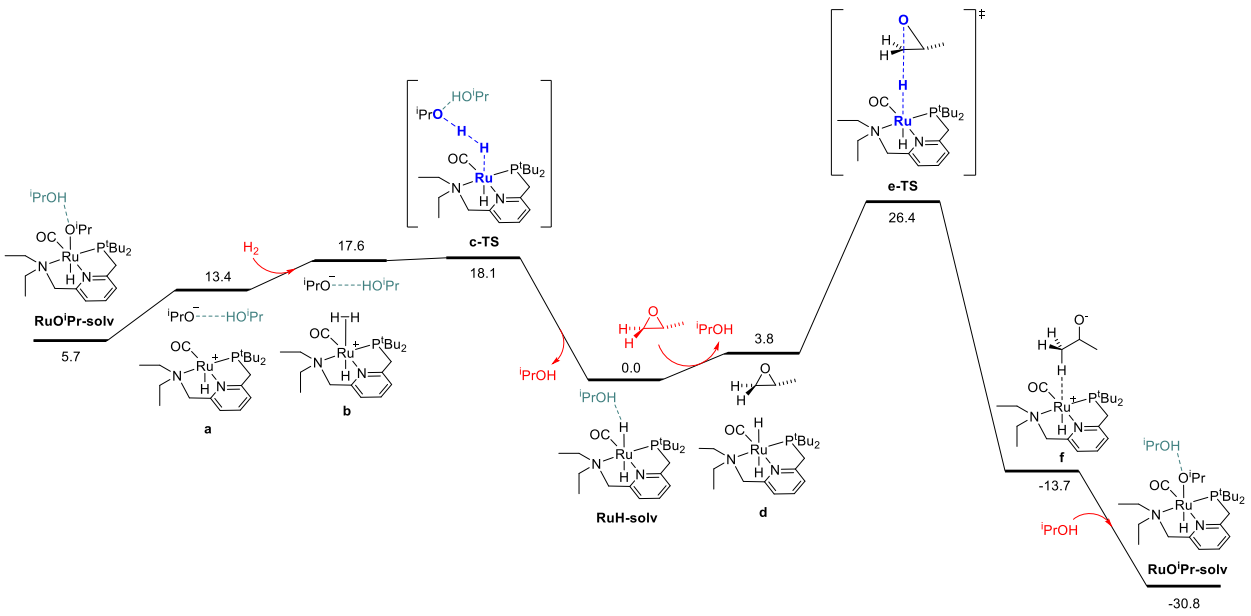


**Figure 2.** Minimum-energy pathway for epoxide hydrogenolysis beginning with **RuO$^i$Pr-solv**. Atoms in bold and blue represent the atoms primarily involved in bond-breaking and bond-forming in transition states. The energies reported are Gibbs free energies at the 298.15 K, corrected to the 1.0 M standard state for all species except for the solvent isopropyl alcohol, whose standard state is 13.08 M, its neat molarity. Mass balance is ensured throughout, and energies are calculated relative to **RuH-solv**, the main catalyst resting state.

Because **e-TS** features a developing negative charge on the epoxide oxygen, we modeled this pathway including an explicit molecule of isopropyl alcohol to stabilize this negative charge through hydrogen bonding. This pathway, shown in Figure S5, had a slightly higher barrier of 26.7 kcal/mol. In contrast, the activation of hydrogen via **c-TS** does require the explicit isopropyl alcohol molecule shown in Figure 2; the analogous pathway without explicit solvent proceeded through a transition-state **k-TS** that was 6.2 kcal/mol higher in free energy (Figure S6). As hydrogen activation involving the pincer $CH_2$ linkers has featured prominently in previous DFT studies on Milstein's catalyst,[17b, 17d, 17e, 17g, 17h, 23] we considered these pathways as alternatives to the MEP shown in Figure 2. We located $H_2$ activation transition states involving either **Ru-dearom** or its isomer where the $NCH_2$ linker is deprotonated, in both cases including an isopropyl alcohol molecule as proton shuttle. These pathways, shown in figures S7 and S8 in the Supporting Information, proceed through barriers at least 7.4 kcal/mol higher than the alkoxide-mediated mechanism through **f-TS**.

### Predicted Kinetics

For the MEP shown in Figure 2, the reaction kinetics can be simplified as shown below in Scheme 7. The hydridoalkoxide **RuO$^i$Pr** and the dihydride **RuH** first establish a rapid pre-equilibrium, which is followed by rate-limiting epoxide ring-opening through **e-TS**.

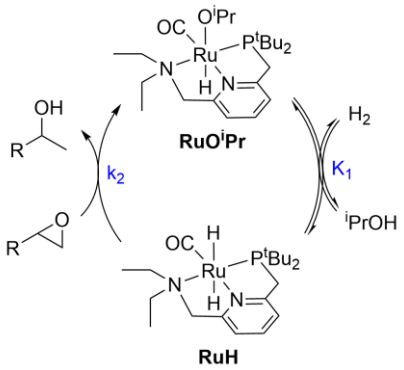


**Scheme 7.** Simplified mechanism determining the kinetics for epoxide hydrogenolysis.

As derived in the Supporting Information, this scheme leads to the following rate law:

$$\text{rate} = k_2[\mathbf{RuH}] = \frac{k_2[\text{Ru}]_{\text{total}}[\text{H}_2][\text{epoxide}]}{[\text{H}_2] + \frac{1}{K_1}}$$

The rate is expected to vary in a first-order manner with the total ruthenium concentration and the epoxide concentration. The dependence of the rate on the hydrogen pressure is expected to follow saturation kinetics, exhibiting first-order dependence at low hydrogen pressure and zero-order dependence at higher pressure. In the kinetics experiments described below, the hydrogen pressures employed range from 10 bar to 30 bar. Based on the experimentally measured $K_1$ value of 89 (see above), this leads to predicted mole fractions [**RuH**]/$[\text{Ru}]_{\text{total}}$ ranging from 0.76 to 0.90. Because the Scheme 7 pre-equilibrium is already shifted mostly toward **RuH** under these conditions, only a modest effect of $P_{H2}$ on the catalytic rate is expected.

**Kinetic Studies**

We then sought to experimentally determine the effects of reactant and catalyst concentrations on the reaction rate, to compare with the predictions from computation. For kinetic studies, we monitored the hydrogenolysis of racemic 1-tetradecene oxide with varying concentrations of epoxide, ruthenium, and base, as well as varying hydrogen pressure. We chose 1-tetradecene oxide as the substrate for several reasons: 1) the reaction is very clean, as branched 2-tetradecanol is the only observed product; 2) low volatility of the reactant and product facilitate accurate quantitation; and 3) it is sterically very similar to propylene oxide, which was used in the computational studies as described above. We used KO$^i$Pr as base rather than KO$^t$Bu, to avoid potential complications resulting from mixtures of alcohols and alkoxide anions in solution.

In the standard experiment, 1-tetradecene oxide (0.25 M), **RuCl** (0.005 M), and KO$^i$Pr (0.0188 M) were stirred at 25 °C for four hours under 20 bar of hydrogen, and the reaction progress was monitored by gas chromatography (Scheme 8). In all kinetic experiments, the epoxide was consumed in a pseudo-first-order manner after an induction period of approximately 15-30 minutes (See Table S5 for complete data). At this point, we do not have a clear explanation for these brief induction periods, but we suspect

they may arise from the heterogeneous nature of the activation of **RuCl** by KO$^i$Pr, which results in precipitation of KCl. In the plots below, $k_{obs}$ is calculated from the slope of the plot of ln[epoxide] vs. time, excluding data from the first 30 minutes of reaction.

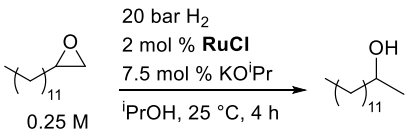


**Scheme 8.** Standard conditions for kinetic experiments

First, we examined the effect of the concentration of the precatalyst, **RuCl**. As Figure 3a shows, $k_{obs}$ increases linearly with $[Ru]_{total}$, consistent with a first-order dependence of the rate on $[Ru]_{total}$. This suggests a monomeric active catalyst species, consistent with the DFT calculations described above. Next, we varied the initial concentration of the epoxide, 1-tetradecene oxide. As Figure 3b shows, a minimal effect on $k_{obs}$ is observed, consistent with minimal saturation in [epoxide] or product inhibition. We then monitored the reaction under different pressures of hydrogen (Figure 3c). The slight increase in $k_{obs}$ with increasing hydrogen pressure agrees remarkably well with the above measurements of the equilibrium between the two resting states **RuO$^i$Pr** and **RuH**. Essentially, the increase in $k_{obs}$ arises from a higher steady-state mole fraction of **RuH** at higher hydrogen pressures, which increases from 0.76 at 10 bar to 0.90 at 30 bar. Last, we observed a slight but consistent increase in $k_{obs}$ with increasing [KO$^i$Pr] (Figure 3d). As described above, the alkoxide base is not involved in the turnover-frequency-determining sequence from **RuH** to **e-TS**, and is not expected to affect the reaction rate based on the calculated minimum-energy pathway. Further investigations into this effect are described in the next section.

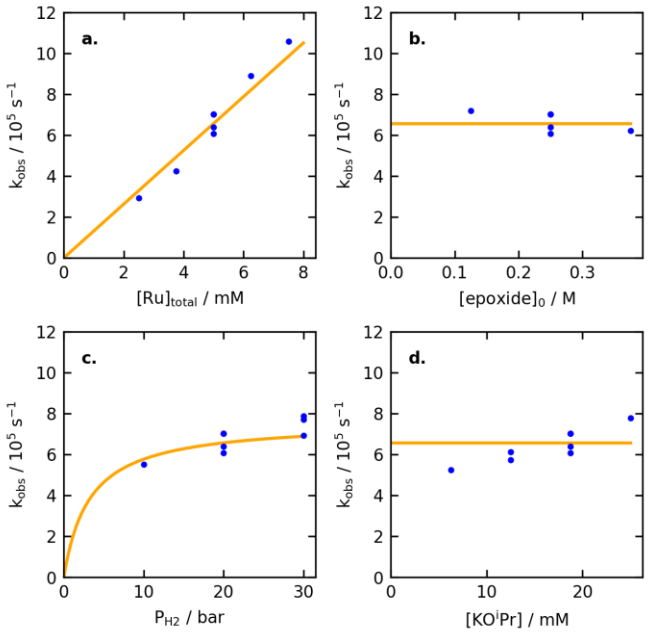


**Figure 3.** Plots of $k_{obs}$ vs $[Ru]_{total}$ (a), $[epoxide]_0$ (b), hydrogen pressure (c), and $[KO^iPr]$ (d). Blue points represent $k_{obs}$ values from independent experiments. Orange lines represent the $k_{obs}$ value predicted from a global fit of all 18 experiments.

Using the above overall rate law and the $K_1$ value of 89 ± 6 determined from NMR experiments, we calculated $k_2$ as 0.0152 ± 0.0016 $M^{-1}{\cdot}s^{-1}$ (see the SI for details). Applying the Eyring equation at 298.15 K gives an activation free energy $\Delta G^{\ddagger}$ of 19.93 ± 0.06 kcal/mol for this step. This experimental barrier, which corresponds to the free energy difference between **RuH-solv** and **e-TS** in Figure 2, is somewhat lower than the barrier of 26.4 kcal/mol calculated by DFT, which may reflect an incomplete modeling of the beneficial effect of the alkoxide base in catalysis, as described in more detail below.

**Effect of the alkali metal cation and added [2.2.2]cryptand.**

Because of the notable effect of the alkali metal cation on product yield during catalyst optimization ($K^+ > Na^+ > Li^+$, Table 1, Entries 22-24), as well as the modest increase in reaction rate with increasing $KO^iPr$ concentration (Figure 3d), we decided to examine the rate of epoxide hydrogenolysis with $NaO^iPr$, compared to the optimal base $KO^iPr$. To attempt to deconvolute potential activating vs inhibiting effects of the metal cation, we measured the reaction rate for both bases in the presence of varying amounts of [2.2.2]cryptand, which sequesters both cations strongly in alcohol solvents.[24] Figure 4 shows the dependence of $k_{obs}$ on the concentration of added cryptand for both bases.

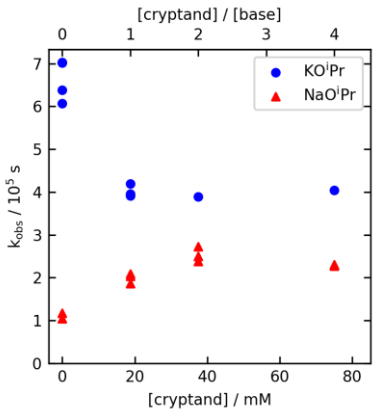


**Figure 4.** Dependence of $k_{obs}$ on the concentration of added [2.2.2]cryptand for epoxide hydrogenolysis with 18.75 mM KO$^i$Pr (blue circles) or NaO$^i$Pr (red triangles).

First, it is notable that, in the absence of added cryptand, the rate of epoxide hydrogenolysis is approximately six times larger for KO$^i$Pr vs. NaO$^i$Pr. This is consistent with the results from optimization (Table 1, Entries 23 vs. 24). The addition of cryptand slows the reaction with KO$^i$Pr and accelerates the reaction with NaO$^i$Pr, bringing the $k_{obs}$ values closer to one another. Empirically, this points to a reactivity order $Na^+$ < [M-cryptand]$^+$ < $K^+$.

A recent review by Dub summarizes some of the potential causes for the beneficial effect of metal-alkoxides in Noyori-type hydrogenation catalysis.[25] Possible effects of the metal alkoxide include catalyst activation through deprotonation of an acidic site (e.g. replacing N-H with N-K),[26] substrate activation where a metal alkoxide cluster stabilizes a developing negative charge on a substrate oxygen,[27] and reactivation of catalysts deactivated by trace water.[28] Further complicating the magnitude of the effect, metal alkoxides are known to aggregate into variably sized clusters in alcohol solvents, which changes the effective concentration of both the alkoxide anion and the metal cation.[25] Pidko, Filonenko, and coworkers recently described a detailed study of the effects of KO$^t$Bu concentration on ester hydrogenation catalyzed by a Noyori-type Mn-pincer catalyst.[29] In their system, the reaction rate is higher at higher base concentration, and they applied the COSMO-RS solvation model to show that the base concentration affects the free energies of on- and off-cycle Mn species, with the net effect that inhibition by the primary alcohol product is reduced at higher [KO$^t$Bu]. In our system, the data do not clearly distinguish between these potential effects. We hesitate to draw conclusions from further computation, as even the sixfold increase in reaction rate for KO$^i$Pr vs. NaO$^i$Pr amounts to only a 1.1 kcal/mol decrease in the overall free-energy barrier for catalysis at 25 °C.

## Summary and Conclusion

In this work, we report the first example of a homogeneous catalyst for the selective formation of highly enantiomerically enriched secondary alcohols via hydrogenolysis of epoxides. The development of the optimized **RuCl**/KO$^t$Bu catalyst system, which minimizes product racemization, was substantially informed by previous mechanistic work in our group. In particular, the insight that epoxide ring-opening

mediated by ruthenium-hydrides does not require a Noyori-type Ru-H/N-H unit[14] spurred us to focus our screening on catalysts lacking an N-H group, as shown in Tables 1 and S1. The knowledge that the PNN- and CNN-pincer-ruthenium complexes shown in Table 1 (Entries 1-5), when activated by base, convert to N-H-containing catalysts at elevated temperatures[13] informed the decision to screen catalysts at room temperature.

For the optimized catalyst system, our proposed mechanism is based on a detailed experimental/computational study. In the MEP calculated by DFT, heterolytic hydrogen activation is mediated by the ruthenium center and exogenous alkoxide base, as previously proposed by Gusev.[20] Epoxide ring-opening is facilitated by $S_N2$-like attack of the ruthenium-hydride on the less-hindered epoxide carbon. The calculated MEP led to predictions for hydrogen-pressure-dependent catalyst speciation, validated experimentally by NMR measurements, and an overall rate law for catalysis validated experimentally by kinetics.

## Author Information

### Corresponding Authors

*jkeith@colgate.edu
*achianese@colgate.edu

### ORCID

Olivia J. Borden: 0000-0002-5567-3566
Benjamin T. Joseph: 0000-0003-2563-1928
Marianna C. Head: 0000-0002-7158-6630
Diane Eun Kim: 0009-0000-6582-3153
Abigail C. Bonino: 0009-0002-7131-0279
Jason M. Keith: 0000-0002-5292-397X
Anthony R. Chianese: 0000-0002-9140-6115

### Supporting Information

Experimental and computational details (PDF). Atomic coordinates (XYZ) for all computed molecular structures, compiled as one file readable by the free program Mercury[30].

### Author Contributions

O. J. Borden: catalyst discovery and optimization, substrate scope. B. T. Joseph: DFT calculations. M. C. Head: kinetic experiments, NMR study of catalyst speciation. Obsidian Ammons: Kinetic experiments. D. E. Kim: substrate scope. A. C. Bonino: substrate scope. J. M. Keith: funding acquisition, supervision of computational work, review and editing of manuscript. A. R. Chianese: conceptualization, funding acquisition, supervision, writing and editing of manuscript.

## Conflicts of interest

The authors declare no competing financial interest.


## Acknowledgements

We thank the National Science Foundation (CHE-2247229) for support of this research project.


## References


(1) Ito, M.; Hirakawa, M.; Osaku, A.; Ikariya, T. Highly Efficient Chemoselective Hydrogenolysis of Epoxides Catalyzed by a ($\eta^5$-$C_5(CH_3)_5$)Ru Complex Bearing a 2-(Diphenylphosphino)Ethylamine Ligand. *Organometallics* **2003,** *22*, 4190-4192.

(2) Rainsberry, A. N.; Sage, J. G.; Scheuermann, M. L. Iridium-Promoted Conversion of Terminal Epoxides to Primary Alcohols under Acidic Conditions Using Hydrogen. *Catal. Sci. Technol.* **2019,** *9*, 3020-3022.

(3) Gitnes, R. M.; Wang, M.; Bao, Y.; Scheuermann, M. L. In Situ Generation of Catalytically Relevant Nanoparticles from a Molecular Pincer Iridium Precatalyst During Polyol Deoxygenation. *ACS Catal.* **2021,** *11*, 495-501.

(4) Yao, C.; Dahmen, T.; Gansäuer, A.; Norton, J. Anti-Markovnikov Alcohols Via Epoxide Hydrogenation through Cooperative Catalysis. *Science* **2019,** *364*, 764-767.

(5) Liu, W.; Li, W.; Spannenberg, A.; Junge, K.; Beller, M. Iron-Catalysed Regioselective Hydrogenation of Terminal Epoxides to Alcohols under Mild Conditions. *Nature Catalysis* **2019,** *2*, 523-528.

(6) Liu, W.; Leischner, T.; Li, W.; Junge, K.; Beller, M. A General Regioselective Synthesis of Alcohols by Cobalt-Catalyzed Hydrogenation of Epoxides. *Angew. Chem. Int. Ed.* **2020,** *59*, 11321-11324.

(7) Noyori, R.; Ohkuma, T. Asymmetric Catalysis by Architectural and Functional Molecular Engineering: Practical Chemo- and Stereoselective Hydrogenation of Ketones. *Angew. Chem. Int. Ed.* **2001,** *40*, 40-73.

(8) Thiyagarajan, S.; Gunanathan, C. Ruthenium-Catalyzed Selective Hydrogenation of Epoxides to Secondary Alcohols. *Org. Lett.* **2019,** *21*, 9774-9778.

(9) Tadiello, L.; Gandini, T.; Stadler, B. M.; Tin, S.; Jiao, H.; de Vries, J. G.; Pignataro, L.; Gennari, C. Regiodivergent Reductive Opening of Epoxides by Catalytic Hydrogenation Promoted by a (Cyclopentadienone)Iron Complex. *ACS Catal.* **2021,** *12*, 235-246.

(10) Ito, M.; Ikariya, T. Catalytic Hydrogenation of Polar Organic Functionalities Based on Ru-Mediated Heterolytic Dihydrogen Cleavage. *Chem. Commun.* **2007**, 5134-42.

(11) Kirlin, F. L.; Borden, O. J.; Head, M. C.; Kelly, S. E.; Chianese, A. R. Epoxide Hydrogenolysis Catalyzed by Ruthenium PNN and PNP Pincer Complexes. *Organometallics* **2022,** *41*, 1025-1033.

(12) Zhang, J.; Leitus, G.; Ben-David, Y.; Milstein, D. Facile Conversion of Alcohols into Esters and Dihydrogen Catalyzed by New Ruthenium Complexes. *J. Am. Chem. Soc.* **2005,** *127*, 10840-10841.

(13) He, T.; Buttner, J. C.; Reynolds, E. F.; Pham, J.; Malek, J. C.; Keith, J. M.; Chianese, A. R. Dehydroalkylative Activation of CNN- and PNN-Pincer Ruthenium Catalysts for Ester Hydrogenation. *J. Am. Chem. Soc.* **2019,** *141*, 17404-17413.

(14) Head, M. C.; Joseph, B. T.; Keith, J. M.; Chianese, A. R. The Mechanism of Markovnikov-Selective Epoxide Hydrogenolysis Catalyzed by Ruthenium PNN and PNP Pincer Complexes. *Organometallics* **2023,** *42*, 347-356.

(15) (a) Gunanathan, C.; Ben-David, Y.; Milstein, D. Direct Synthesis of Amides from Alcohols and Amines with Liberation of $H_2$. *Science* **2007,** *317*, 790-792. (b) Gnanaprakasam, B.; Ben-David, Y.; Milstein, D. Ruthenium Pincer-Catalyzed Acylation of Alcohols Using Esters with Liberation of Hydrogen under Neutral Conditions. *Adv. Synth. Catal.* **2010,** *352*, 3169-3173. (c) Balaraman, E.; Gunanathan, C.; Zhang, J.; Shimon, L. J. W.; Milstein, D. Efficient Hydrogenation of Organic Carbonates, Carbamates and Formates Indicates Alternative Routes to Methanol Based on $CO_2$ and CO. *Nature Chem.* **2011,** *3*, 609-614. (d) Gnanaprakasam, B.; Balaraman, E.; Ben-David, Y.; Milstein, D. Synthesis of Peptides and Pyrazines from Beta-Amino Alcohols through Extrusion of $H_2$ Catalyzed by Ruthenium Pincer Complexes: Ligand-Controlled Selectivity. *Angew. Chem. Int. Ed.* **2011,** *50*, 12240-12244. (e) Gnanaprakasam, B.; Milstein, D. Synthesis of Amides from Esters and Amines with Liberation of $H_2$ under Neutral Conditions. *J. Am. Chem. Soc.* **2011,** *133*, 1682-1685. (f) Zeng, H.; Guan, Z. Direct Synthesis of Polyamides Via Catalytic Dehydrogenation of Diols and Diamines. *J. Am. Chem. Soc.* **2011,** *133*, 1159-1161. (g) Rigoli, J. W.; Moyer, S. A.; Pearce, S. D.; Schomaker, J. M. Alpha,Beta-Unsaturated Imines Via Ru-Catalyzed Coupling of Allylic Alcohols and Amines. *Org. Biomol. Chem.* **2012,** *10*, 1746-1749. (h) Huff, C. A.; Sanford, M. S. Catalytic $CO_2$ Hydrogenation to Formate by a Ruthenium Pincer Complex. *ACS Catal.* **2013,** *3*, 2412-2416. (i) Chaudhari, M. B.; Bisht, G. S.; Kumari, P.; Gnanaprakasam, B. Ruthenium-Catalyzed Direct Alpha-Alkylation of Amides Using Alcohols. *Org. Biomol. Chem.* **2016,** *14*, 9215-9220.

(16) Zhang, J.; Leitus, G.; Ben-David, Y.; Milstein, D. Efficient Homogeneous Catalytic Hydrogenation of Esters to Alcohols. *Angew. Chem. Int. Ed.* **2006,** *45*, 1113-1115.

(17) (a) Yang, X.; Hall, M. B. Mechanism of Water Splitting and Oxygen-Oxygen Bond Formation by a Mononuclear Ruthenium Complex. *J. Am. Chem. Soc.* **2010,** *132*, 120-130. (b) Li, H.; Wang, X.; Huang, F.; Lu, G.; Jiang, J.; Wang, Z.-X. Computational Study on the Catalytic Role of Pincer Ruthenium(II)-PNN Complex in Directly Synthesizing Amide from Alcohol and Amine: The Origin of Selectivity of Amide over Ester and Imine. *Organometallics* **2011,** *30*, 5233-5247. (c) Sandhya, K. S.; Suresh, C. H. Water Splitting Promoted by a Ruthenium(II) PNN Complex: An Alternate Pathway through a Dihydrogen Complex for Hydrogen Production. *Organometallics* **2011,** *30*, 3888-3891. (d) Zeng, G.; Li, S. Insights into Dehydrogenative Coupling of Alcohols and Amines Catalyzed by a (PNN)-Ru(II) Hydride Complex: Unusual Metal-Ligand Cooperation. *Inorg. Chem.* **2011,** *50*, 10572-10580. (e) Li, H.; Wen, M.; Wang, Z.-X. Computational Mechanistic Study of the Hydrogenation of Carbonate to Methanol Catalyzed by the (RuPNN)-P-II Complex. *Inorg. Chem.* **2012,** *51*, 5716-5727. (f) Ma, C.; Piccinin, S.; Fabris, S. Reaction Mechanisms of Water Splitting and $H_2$ Evolution by a Ru(II)-Pincer Complex Identified with Ab Initio Metadynamics Simulations. *ACS Catal.* **2012,** *2*, 1500-1506. (g) Yang, X. Metal Hydride and Ligand Proton Transfer Mechanism for the Hydrogenation of Dimethyl Carbonate to Methanol Catalyzed by a Pincer Ruthenium Complex. *ACS Catal.* **2012,** *2*, 964-970. (h) Cho, D.; Ko, K. C.; Lee, J. Y. Catalytic Mechanism for the Ruthenium-Complex-Catalyzed Synthesis of Amides from Alcohols and Amines: A DFT Study. *Organometallics* **2013,** *32*, 4571-4576. (i) Hasanayn, F.; Baroudi, A.; Bengali, A. A.; Goldman, A. S. Hydrogenation of Dimethyl Carbonate to Methanol by Trans-$[Ru(H)_2(PNN)(CO)]$ Catalysts: DFT Evidence for Ion-Pair-Mediated Metathesis Paths for C–OMe Bond Cleavage. *Organometallics* **2013,** *32*, 6969-6985. (j) Sandhya, K. S.; Remya, G. S.; Suresh, C. H. Pincer Ligand Modifications to Tune the Activation Barrier for $H_2$ Elimination in Water Splitting Milstein Catalyst. *Inorg Chem* **2015,** *54*, 11150-11156. (k) Li, L.; Lei, M.; Liu, L.; Xie, Y.;

Schaefer, H. F. Metal-Substrate Cooperation Mechanism for Dehydrogenative Amidation Catalyzed by a PNN-Ru Catalyst. *Inorg. Chem.* **2018,** *57*, 8778-8787.
(18) Pham, J.; Jarczyk, C. E.; Reynolds, E. F.; Kelly, S. E.; Kim, T.; He, T.; Keith, J. M.; Chianese, A. R. The Key Role of the Latent N–H Group in Milstein's Catalyst for Ester Hydrogenation. *Chem. Sci.* **2021,** *12*, 8477-8492.
(19) Dawe, L. N.; Karimzadeh-Younjali, M.; Dai, Z.; Khaskin, E.; Gusev, D. G. The Milstein Bipyridyl PNN Pincer Complex of Ruthenium Becomes a Noyori-Type Catalyst under Reducing Conditions. *J. Am. Chem. Soc.* **2020,** *142*, 19510-19522.
(20) Gusev, D. G. Revised Mechanisms of the Catalytic Alcohol Dehydrogenation and Ester Reduction with the Milstein PNN Complex of Ruthenium. *Organometallics* **2020,** *39*, 258-270.
(21) Perdriau, S.; Chang, M. C.; Otten, E.; Heeres, H. J.; de Vries, J. G. Alkene Isomerisation Catalysed by a Ruthenium PNN Pincer Complex. *Chem. Eur. J.* **2014,** *20*, 15434-15442.
(22) Liang, Y.; Luo, J.; Milstein, D. Facile Synthesis of Amides Via Acceptorless Dehydrogenative Coupling of Aryl Epoxides and Amines. *Chem. Sci.* **2022,** *13*, 5913-5919.
(23) (a) Hou, C.; Zhang, Z.; Zhao, C.; Ke, Z. DFT Study of Acceptorless Alcohol Dehydrogenation Mediated by Ruthenium Pincer Complexes: Ligand Tautomerization Governing Metal Ligand Cooperation. *Inorg. Chem.* **2016,** *55*, 6539-6551. (b) Wang, H.; Liu, C.; Zhang, D. Decisive Effects of Solvent and Substituent on the Reactivity of Ru-Catalyzed Hydrogenation of Ethyl Benzoate to Benzyl Alcohol and Ethanol: A DFT Study. *Mol. Catal.* **2017,** *440*, 120-132.
(24) (a) Cox, B. G.; Schneider, H.; Stroka, J. Kinetics of Alkali Metal Complex Formation with Cryptands in Methanol. *J. Am. Chem. Soc.* **1978,** *100*, 4746-4749. (b) Cox, B. G.; Garcia-Rosas, J.; Schneider, H. Solvent Dependence of the Kinetics of Formation and Dissociation of Cryptate Complexes. *J. Am. Chem. Soc.* **1981,** *103*, 1054-1059.
(25) Dub, P. A. Alkali Metal Alkoxides in Noyori-Type Hydrogenations. *Eur. J. Inorg. Chem.* **2021,** *2021*, 4884-4889.
(26) (a) Dub, P. A.; Gordon, J. C. The Role of the Metal-Bound N–H functionality in Noyori-Type Molecular Catalysts. *Nat. Rev. Chem.* **2018,** *2*, 396-408. (b) Dub, P. A.; Henson, N. J.; Martin, R. L.; Gordon, J. C. Unravelling the Mechanism of the Asymmetric Hydrogenation of Acetophenone by [$RuX_2$(Diphosphine)(1,2-Diamine)] Catalysts. *J. Am. Chem. Soc.* **2014,** *136*, 3505-3521. (c) Nakane, S.; Yamamura, T.; Manna, S. K.; Tanaka, S.; Kitamura, M. Mechanistic Study of the Ru-Catalyzed Asymmetric Hydrogenation of Nonchelatable and Chelatable Tert-Alkyl Ketones Using the Linear Tridentate $sp^3P/sp^3NH/sp^2N$-Combined Ligand PN(H)N: RuNH- and RuNK-Involved Dual Catalytic Cycle. *ACS Catal.* **2018,** *8*, 11059-11075.
(27) Dub, P. A.; Batrice, R. J.; Gordon, J. C.; Scott, B. L.; Minko, Y.; Schmidt, J. G.; Williams, R. F. Engineering Catalysts for Selective Ester Hydrogenation. *Org. Process Res. Dev.* **2020,** *24*, 415-442.
(28) Nguyen, D. H.; Trivelli, X.; Capet, F.; Swesi, Y.; Favre-Réguillon, A.; Vanoye, L.; Dumeignil, F.; Gauvin, R. M. Deeper Mechanistic Insight into Ru Pincer-Mediated Acceptorless Dehydrogenative Coupling of Alcohols: Exchanges, Intermediates, and Deactivation Species. *ACS Catal.* **2018,** *8*, 4719-4734.
(29) Yang, W.; Kalavalapalli, T. Y.; Krieger, A. M.; Khvorost, T. A.; Chernyshov, I. Y.; Weber, M.; Uslamin, E. A.; Pidko, E. A.; Filonenko, G. A. Basic Promotors Impact Thermodynamics and Catalyst Speciation in Homogeneous Carbonyl Hydrogenation. *J. Am. Chem. Soc.* **2022,** *144*, 8129-8137.
(30) Macrae, C. F.; Edgington, P. R.; McCabe, P.; Pidcock, E.; Shields, G. P.; Taylor, R.; Towler, M.; van de Streek, J. Mercury: Visualization and Analysis of Crystal Structures. *J. Appl. Cryst.* **2006,** *39*, 453-457.

**Table of contents graphic:**

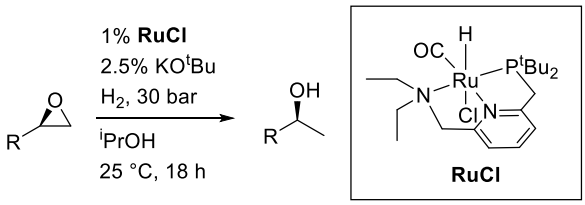


Mechanistic study:

- NMR characterization of resting states
- Rate law and energetic span by kinetics
- Minimum-energy pathway by DFT